Regional climate modeling over the Maritime Continent: Improving representations of boundary layer processes

Rebecca L. Gianotti* **and Elfatih A. B. Eltahir**

Ralph M. Parsons Laboratory, Massachusetts Institute of Technology,

15 Vassar St, Cambridge MA 02139, USA

ELTAHIR Research Group Report #3,
March, 2014

Abstract

This paper describes work to improve the representation of boundary layer processes within a regional climate model (Regional Climate Model Version 3 (RegCM3) coupled to the Integrated Biosphere Simulator (IBIS)) applied over the Maritime Continent. In particular, modifications were made to improve model representations of the mixed boundary layer height and non-convective cloud cover within the mixed boundary layer. Model output is compared to a variety of ground-based and satellite-derived observational data, including a new dataset obtained from radiosonde measurements taken at Changi airport, Singapore, four times per day. These data were commissioned specifically for this project and were not part of the airport's routine data collection. It is shown that the modifications made to RegCM3-IBIS significantly improve representations of the mixed boundary layer height and low-level cloud cover over the Maritime Continent region by lowering the simulated nocturnal boundary layer height and removing erroneous cloud within the mixed boundary layer over land. The results also show some improvement with respect to simulated radiation and rainfall, compared to the default version of the model.

Keywords: mixed boundary layer height, regional climate model, boundary layer cloud, Maritime Continent.

1. Introduction

The skill of large-scale climate models (global, GCMs, and regional, RCMs) in reproducing the existing climate has improved significantly over many parts of the world. However, simulations over the Maritime Continent region still contain substantial error (e.g. Yang and Slingo 2001, Neale and Slingo 2003, Dai and Trenberth 2004, Wang *et al.* 2007). The Fourth Assessment Report of the Intergovernmental Panel on Climate Change (IPCC) noted that projections of future rainfall over the Southeast Asian region, including the Maritime Continent, vary so widely as to disagree on the sign of the change (Christensen *et al.* 2007). This variation indicates that the mechanisms driving rainfall in this region are still not adequately understood or represented in climate models.

The work documented in Gianotti *et al.* (2012) showed that the Regional Climate Model Version 3.0 (RegCM3) exhibited significant error with respect to simulation of the diurnal cycle of rainfall over the Maritime Continent, when coupled with either of the land surface schemes Biosphere Atmosphere Transfer Scheme Version 1e (BATS1e) or Integrated Biosphere Simulator (IBIS). Errors were also documented with respect to net radiation, latent and sensible heat fluxes and evapotranspiration over the land surface (Gianotti *et al.* 2012). The authors noted that the errors exhibited by RegCM3 were not unique to that model but instead were consistent with other published climate modeling studies conducted over the Maritime Continent region (e.g. Chow *et al.* 2006, Francisco *et al.* 2006, Martin *et al.* 2006, Wang *et al.* 2007).

It was argued that the source of the errors resided primarily in the atmospheric component of the RegCM3 coupled model system, specifically with the simulation of convective rainfall, and that two avenues of research might be pursued to address the simulated rainfall errors: 1) simulation of the mixed planetary boundary layer and the diurnal processes that create instability in the near surface environment, and 2) threshold criteria for triggering of convection (Gianotti *et al.* 2012). This paper investigates and modifies representation of the mixed boundary layer within the RegCM3-IBIS coupled model system. Particular attention is paid to simulation of the mixed boundary layer height and non-convective clouds within the mixed boundary layer.

a. Height of the Mixed Boundary Layer

Most GCMs and RCMs use a parameterization scheme to describe the evolution of thermodynamic properties in the lower atmosphere due to turbulent transport within the mixed boundary layer and entrainment of air from above the mixed boundary layer. The height of the turbulently-mixed boundary layer is a key variable since it separates the free-atmosphere, laminar, resolved flow from the near-surface, turbulent, parameterized flow. However, to the best of our knowledge, the simulated boundary layer height within RegCM3 has not been evaluated against observational data. In general, simulations of boundary layer height are rarely evaluated within climate models (Seidel *et al*. 2012), even though some modeling studies have shown a very sensitive response of precipitation to the depth of the mixed boundary layer (e.g. Cha *et al.* 2008).

One particular modeling challenge is representation of the nocturnal stable layer. Parameterization schemes similar to that used in RegCM3 (described below in the Methodology section) do not explicitly resolve the details of the diurnally-varying boundary region – there is no defined residual layer, and there is no distinct representation of a stable layer that develops from the ground upwards beneath the residual layer. Instead, the model attempts to separate a layer that is mixed from a free atmosphere.

However, the nocturnal stable layer has a poorly-defined top that blends into the residual layer (Stull 1988). Tombrou *et al.* (1998) noted that, "although a lot of studies have been devoted to [the height of the nocturnal PBL], there is still confusion in the definition of its upper boundary and thus the determination of its depth." The modeling challenge then is how to estimate the depth of a near-surface layer at night that experiences turbulent but not convective mixing.

Ziilitinkevich and Baklanov (2002) reviewed the most common approaches to estimating the stable boundary layer height, including: various methods for utilizing the critical Richardson number (gradient, bulk and finite-difference versions among them); static stability above the boundary layer as measured by the Brunt-Väisälä frequency; and diagnostic multi-limit equations derived from the turbulent kinetic energy budget and momentum equations. All of these relationships depend on specification of the Coriolis parameter, f. The diagnostic relationship employed in RegCM3, which is described in Vogelezang and Holtslag (1996), is also dependent upon the Coriolis parameter.

Unfortunately, as noted by Zilitinkevich and Baklanov (2002), many of these methods are not applicable to the equatorial stable boundary layer because of the tendency for $f \rightarrow 0$ over the tropics, which leads to either unlimited growth of the boundary layer or a singularity (depending on whether the height is directly or inversely proportional to f). It was noted by Vogelezang and Holtslag (1996) that the diagnostic relationship used within their scheme is only applicable outside the tropics, even though it is applied over all potential model domains within RegCM3.

Instead, Zilitinkevich and Baklanov (2002) note that a climatological upper limit $h \leq h^*$ should be placed on the equatorial stable boundary layer. However, this upper limit remains problematic since it has been established that the boundary layer height limit varies by geographic region (Zilitinkevich and Baklanov 2002).

Joffre *et al*. (2001) showed that other non-rotational relationships (i.e. those not dependent on the Coriolis parameter) could be used as part of the stable boundary layer determination, such as the length scale $L_N = u^*/N$, where u^* is the surface frictional velocity and N is the Brunt-Väisälä frequency. However, Vogelezang and Holtslag (1996) showed that their method for estimating the boundary layer height using the critical Richardson number could be reduced to the same length scale using L_N, for certain values of the coefficients, and therefore this relationship does not add any new information to the search for a robust stable boundary layer height over the tropics.

Two empirical expressions for the stable boundary layer height that depend only on the velocity at 10 m above the surface were also noted by Zilitinkevich and Baklanov (2002). However, those authors noted that these two expressions contain large biases and root mean squared errors, and therefore are also not satisfactory.

Hence a robust definitive expression for the equatorial nocturnal stable layer is still lacking. In this work, we compare the mixed boundary layer height simulated by RegCM3 to an observational dataset acquired over the Maritime Continent, and present modifications to improve the representation of this height in the model.

b. Non-convective Clouds in the Mixed Boundary Layer

Cumulus and stratocumulus clouds can form near the top of the mixed boundary layer. These clouds are most commonly observed over subtropical marine regions, particularly off the western coasts of the American continents, and are known to play a crucial role in climate sensitivity (Bachiochi and Krishnamurti 2000, McCaa and Bretherton 2004, Bony and Dufresne 2005). This has been the motivation of several field campaigns – including the First International Satellite Cloud Climatology Project (ISCCP) Regional Experiment (FIRE; Albrecht *et al*. 1988), the Atlantic Stratocumulus Transition Experiment (ASTEX; Albrecht *et al*. 1995), the East Pacific Investigation of Climate (EPIC) model (Bretherton *et al*. 2004), the Second Dynamics and Chemistry of Marine Stratocumulus field study (DYCOMS-II; Stevens *et al*. 2003), and Rain in Shallow Cumulus over the Ocean (RICO; Rauber *et al*. 2007) – as well as extensive modeling

activities (e.g., Krueger *et al*. 1995, Bretherton *et al*. 1999, Svensson *et al*. 2000, McCaa and Bretherton 2004) (as summarized in Karlsson *et al.* 2010).

In the Fourth IPCC Assessment Report (Christensen *et al.* 2007), cloud feedbacks were identified as a primary reason for differences between models, with the shortwave impact of boundary-layer and mid-level clouds making the largest contribution. But their simulation has remained problematic for large-scale climate models (e.g., Bachiochi and Krishnamurti 2000, Bony and Dufresne 2005). Most commonly, coupled GCMs underestimate the presence of low-level marine stratus cloud cover (e.g., Frey *et al.*1997).

To the best of our knowledge, there is no published assessment of cloud cover within the mixed boundary layer region as simulated by RegCM3. However, a tunable parameter exists in RegCM3 that prevents low-level clouds from being radiatively-active, such that these clouds produce rainfall but do not absorb or reflect radiation. The existence of this model parameter suggests that low-level cloud cover has previously been identified as a problem but not adequately addressed.

One published work was found that alludes to use of this parameter. Sun *et al*. (1999) used RegCM2 to simulate rainfall-generation processes over eastern Africa. Part of that work included specifying the cloud base level with respect to the radiation transfer scheme. No further details were given in that work, but we consider it likely that specifying the cloud base involved tuning the parameter governing the elevation of radiatively-active clouds. Sun *et al*. (1999) found that model performance was improved with respect to wind shear

and rainfall when the lowest three model layers were designated cloud-free, instead of just the lowest model layer (the default parameter setting). This work, although somewhat vague, suggests that the simulation of clouds within the mixed boundary layer can have a significant impact.

There are indications that other models may exhibit issues with simulated cloud cover within the PBL. Bachiochi and Krishnamurti (2000) placed constraints on the formation of stratus clouds within the PBL in the Florida State University coupled ocean-atmosphere model. In their case, the goal was to increase the fractional cloud cover over subtropical ocean regions by making the cloud cover a function of the simulated PBL height and ground wetness (Bachiochi and Krishnamurti 2000). Additionally, the cloud fraction was set to zero if the relative humidity was less than 80% at either the PBL top or the model level just below the PBL top (Bachiochi and Krishnamurti 2000). The new cloud fraction was found to greatly improve the simulated cloud amount over the eastern ocean basin, with subsequent improvement in the representation of surface solar radiation fluxes, low-level winds and thermal structure (Bachiochi and Krishnamurti 2000).

In the work of Smith (1990), which is the basis for cloud simulation in the Hadley Centre's Global Environment Model (HadGEM1; Martin *et al.* 2006), a threshold relative humidity value was imposed on the simulation of resolvable (non-convective) cloud, which varied over the PBL: a threshold value of 0.925 was required in the lowest 2 model layers while a value of 0.85 was required in all other model layers. This variable threshold restricts the formation of cloud within the PBL except in the layer directly beneath the PBL top, where

capping stratocumulus cloud is observed to exist. The use of a higher threshold within the PBL is suggestive of an attempt to reduce very low cloud cover.

In NCAR's Community Atmosphere Model Version 4.0 (CAM4.0; Neale *et al.* 2010), the simulation of stratus clouds over marine areas was altered to improve the simulation of subtropical marine stratocumulus cloud. In CAM4.0, stratus cloud over oceans is assumed to be located in the model layer directly beneath the strongest stability jump between 750 mb and the surface (Neale *et al.* 2010), where stability is defined by the gradient in potential temperature. This location represents the model layer below the inversion that signifies the top of the PBL. If no two layers present a potential temperature difference greater than 0.125 K mb^{-1}, no cloud is diagnosed (Neale *et al.* 2010). This limitation would effectively restrict the formation of cloud over ocean grid cells within well-mixed boundary layers.

In this work, we present a new method for representing the formation of non-convective clouds within the mixed boundary layer, which accounts for the impact of turbulent mixing on the vertical distribution of condensate.

2. Methodology

a. Model Description

This work uses the same version of the Regional Climate Model Version 3 (RegCM3) coupled to Integrated Biosphere Simulator (IBIS) as described in Gianotti *et al*. (2012) and Winter *et al.* (2009), including the Subgrid Explicit Moisture Scheme (SUBEX; Pal *et al.*

2000) for resolvable, non-convective clouds and precipitation, the choice of Grell (Grell 1993) with Fritsch-Chappell (Fritsch and Chappell 1980) or Arakawa-Schubert (Grell *et al*. 1994) closures, and Emanuel (Emanuel 1991, Emanuel and Zivkovic-Rothman 1999) convective parameterization schemes. Further details of the developments and description of RegCM3 are available in Pal *et al*. (2007). Only the IBIS land surface scheme is used in this work, since it shows better simulation of the surface fluxes over the Maritime Continent than BATS1e (as shown in Gianotti *et al.* 2012), and its two-layer canopy is a more reasonable representation of the tropical forest within the Maritime Continent region than the one-layer canopy of BATS1e.

Giorgi *et al.* (2012) describes upgrades that were incorporated into a more recent version of RegCM: Version 4 (RegCM4), which was made publicly available in 2011. Aspects of RegCM4 that are relevant to this work are described below.

b. Existing and Proposed Parameterization Schemes

(i) Modifications to Representation of Boundary Layer Height

Two modifications were made to the representation of boundary layer height within RegCM3, which uses the non-local diffusion scheme developed by Holtslag *et al.* (1990) and Holtslag and Boville (1993) (hereafter referred to as 'the Holtslag scheme').

The first of these modifications was to upgrade the Holtslag scheme based on the work of Vogelezang and Holtslag (1996).

In the original Holtslag scheme, the PBL height, h, is solved iteratively from a bulk value of the critical Richardson number, Ri_c:

$$Ri_c = \frac{(g/\theta_{v0})(\theta_{vh} - \theta_{v0})h}{u_h^2 + v_h^2} \quad (1)$$

where $Ri_c = 0.25$, g = gravitational acceleration, θ_v = virtual potential temperature, u = zonal wind component, v = meridional wind component and h = PBL height. The subscript *0* corresponds to the near surface value. The bulk Richardson number Ri is calculated over the level closest to the surface and subsequent higher levels. Once the bulk Ri exceeds Ri_c, the value of PBL height h is derived with a linear interpolation between the layer with $Ri > Ri_c$ and the layer with $Ri < Ri_c$.

To achieve better simulation of the PBL height in neutral and stable conditions, Vogelezang and Holtslag (1996) revised the Holtslag scheme to make it more generally applicable. In the revised scheme, the bulk critical Richardson number, Ri_c, is a function of the wind shear over the depth of the PBL as well as the surface friction velocity:

$$Ri_c = \frac{(g/\theta_{vs})(\theta_{vh} - \theta_{vs})(h - z_s)}{(u_h - u_s)^2 + (v_h - v_s)^2 + bu_*^2} \quad (2)$$

where $Ri_c = 0.25$, g = gravitational acceleration, θ_v = virtual temperature, u = zonal wind component, v = meridional wind component, h = PBL height, z = elevation of model layer,

b = 100, u_* = surface frictional velocity, and the subscript s = model layer 20-80 m above the surface.

The second modification made to the Holtslag scheme within RegCM3 concerns the representation of the nocturnal stable boundary layer height. The general PBL height, within both the original Holtslag scheme and the revised version presented by Vogelezang and Holtslag (1996), is constrained by a minimum threshold used as a way to estimate the height of the nocturnal stable boundary layer, as follows:

$$PBL_{\min} = \frac{0.07 u_*}{f} \qquad (3)$$

where u_* = surface frictional velocity and f = Coriolis parameter. The value of f is constrained such that $f_{\min} = 2.546 \times 10^{-5}$ sec^{-1}, which is the value at 10^o latitude. The Holtslag scheme authors do not cite a reference for this specific equation, but presumably it comes from the work of Koracin and Berkowicz (1988). Over the tropical belt 10^{o}S to 10^{o}N, equation (3) results in $PBL_{min} \geq 2749 u_*$. Hence if the friction velocity is of magnitude 0.1-1 m s^{-1} (which tests showed it frequently is over the Maritime Continent region), the mixed boundary layer cannot collapse below a height of about 500 m.

In the absence of a definitive expression for the nocturnal PBL height over the tropics, the simplest reasonable expression was sought for implementation into RegCM3.

Stull (1988) provides examples of different methods for estimating the depth of the nocturnal PBL, including the lowest height at which the lapse rate is adiabatic (i.e. $\Delta\theta / \Delta z = 0$), indicating the top of the stable layer, consistent with condition 1 of Heffter (1980). Analysis of the Changi Airport data showed that the gradient of potential temperature ($\Delta\theta / \Delta z$) often exceeded 0.005 K m^{-1} at very low elevations in the early morning, resulting in an estimated PBL height of less than 100 m. This indicates that the lapse rate over Singapore frequently becomes adiabatic very close to the surface at night.

Therefore the minimum threshold on the PBL height was changed to z_s, the elevation of the lowest model layer. In RegCM3, this layer takes a height of around 40 m. Note that this threshold does not require the nocturnal boundary layer height be as low as 40 m; it simply removes the previous constraint that was a function of the Coriolis parameter, allowing the PBL to collapse lower than 500 m at night. Sensitivity tests showed that the exact magnitude of the minimum PBL height used within RegCM3 did not significantly impact the results so long as the value was on the order of 200 m or less. Therefore it does not appear that 40 m is a limiting constraint.

It is noted that the nocturnal stable layer over the Maritime Continent will likely be shallower than other tropical regions due to the presence of significant cloud cover and a substantial vegetated canopy, both of which limit night-time radiative cooling. Therefore the lowest model layer may not be an appropriate constraint on the nocturnal stable PBL height over other tropical regions. Future work in this field may elucidate a more definitive diagnostic expression or another method that is more generally applicable over the tropics.

RegCM4 contains modifications to the Holtslag scheme that are not included here (Giorgi *et al.* (2012). Specifically, the countergradient transport term for water vapor was completely removed in RegCM4 to reduce an egregious vertical transport of water vapor in the mixed boundary layer. Also, the eddy diffusivity and countergradient terms for all variables were set to zero in the case of very stable conditions, to reduce excessive vertical transport in the case of very stable conditions such as during winter in the northern high latitudes (Giorgi *et al.* 2012). These modifications are not expected to significantly impact the new representation of nocturnal stable layer height or the new representation of non-convective clouds within the mixed boundary layer, as described in this work.

(ii) New Representation of Non-convective Boundary Layer Clouds in RegCM3

A key feature of boundary layer clouds is their location near the top of, rather than within, the mixed boundary layer, hence the commonly-used terms 'cloud-topped boundary layer' and 'stratocumulus-capped boundary layer'. Within the mixed boundary layer, turbulent eddies are very effective at removing gradients of any active or passive quantity within that turbulent flow (Benkley and Schulman 1979), such that conserved variables like potential temperature and humidity are nearly constant with height within the mixed boundary layer (Stull 1988). It is therefore expected that condensate (cloud liquid water) would be similarly well-mixed within this region. Hence if condensate were simulated by a model within the mixed boundary layer, for example in the case of early morning fog, it would be expected that cloudiness would be relatively uniform over the well-mixed region. Here we present a new formulation to account for this mixing.

In RegCM3, cloud fraction within a grid cell can be created by both convective and large-scale (i.e. resolvable, non-convective) processes. Each type of cloud fraction is calculated independently of the other and then the larger of the two values is taken as the grid-cell cloud fraction for radiative transfer calculations. It was determined that the low-level cloud cover currently simulated by RegCM3 over the Maritime Continent is predominately large-scale.

Large-scale cloud fraction, $FC_{L\text{-}S}$, is calculated by the SUBEX routine (Pal *et al*. 2000) as a function of the average grid cell relative humidity, based on the work of Sundqvist (1988):

$$FC_{L-S} = 1 - \sqrt{1 - \frac{RH - RH_{\min}}{RH_{\max} - RH_{\min}}} \qquad (4)$$

where RH_{min} = threshold RH (relative humidity) required for cloud formation and RH_{max} = maximum value that RH can take. In RegCM3, the default values are RH_{max} = 1.01, RH_{min} = 0.8 over land and RH_{min} = 0.9 over ocean. This formula is applied to each grid volume, uniformly over the depth of a grid cell, such that each model layer has a separate calculation of $FC_{L\text{-}S}$.

This representation of large-scale cloud fraction has not been modified in RegCM4 (Giorgi *et al.* 2012).

To address the representation of variable large-scale cloud fraction within the mixed boundary layer in RegCM3, a limitation was placed on the SUBEX routine such that clouds were not permitted to form unless the bulk saturation exceeded a specified threshold, calculated as follows:

$$RH_{bulk} = \frac{q_{bulk}}{q_{s,bulk}} \tag{5}$$

where RH_{bulk} = bulk measure of relative humidity;

$$q_{bulk} = \sum_{z_s}^{z_{PBL}} q(z)\rho(z)\Delta z \tag{6}$$

where q_{bulk} = bulk measure of water vapor mixing ratio over the PBL depth, $q(z)$ = grid-mean water vapor mixing ratio at elevation z, ρ(z) = grid-mean density at elevation z, Δz = thickness of vertical model layer, z_{PBL} = PBL height as calculated by the modified Holtslag scheme described above, z_s = elevation of lowest model layer;

$$q_{s,bulk} = \sum_{z_s}^{z_{PBL}} q_s(z)\rho(z)\Delta z \tag{7}$$

where $q_{s,bulk}$ = bulk measure of saturation mixing ratio over the PBL depth, $q_s(z)$ = grid-mean saturation mixing ratio at elevation z; and

$$FC_{L-S}(z) = 0 \quad \text{if } RH_{bulk} < RH_T \quad \text{for } z_s < z < z_{PBL} \tag{8}$$

where $FC_{L-S}(z)$ = large-scale fractional cloud cover at elevation z and RH_T = threshold bulk relative humidity. The threshold bulk relative humidity, RH_T, was assigned a value of 0.9, which is consistent with the value of RH_{min} used for general calculation of the large-scale fractional cloud cover.

Note that this condition was only placed on the formation of large-scale cloud cover, and not convective, since it was determined that the majority of cloud cover simulated within the PBL region was large-scale.

c. Experimental Design

Simulations were run with RegCM3-IBIS using both the Grell with Fritsch-Chappell closure and Emanuel convection scheme to test the impact of the new parameterization schemes described above. These simulations are labeled 'modified' in the results presented below and are compared to the default version of RegCM3-IBIS ('default').

Three other minor model modifications were made to improve the representation of surface fluxes within RegCM3-IBIS.These changes were motivated by erroneous simulation of turbulent heat fluxes documented in the default version of RegCM3-IBIS (described in Gianotti *et al.* 2012). None of these modifications had significant impacts upon the simulation results, but they are noted here for completeness.

Firstly, the ocean surface roughness length has been changed such that it is also a function of the wind speed at 10 m above the surface, *U*, in addition to the surface frictional velocity and the kinematic viscosity. This change is consistent with the upgrades made to the COARE algorithm Version 3.0 (Fairall *et al.* 2003). Secondly, the calculation of soil thermal conductivity within IBIS was modified to include the heat capacity of air within the soil matrix. This was not included in the original version (Foley *et al.* 1996), which was based on the work of de Vries (1963) assuming saturated soils. Thirdly, the amount of intercepted canopy storage was reduced by 30% to address a bias in the simulated partitioning of total evapotranspiration into transpiration and interception loss (Gianotti *et al.* 2012). These modifications are described in detail in Gianotti (2012).

One final change was made to RegCM3, to permit cloud cover and cloud liquid water to exist within the second model layer from the top of atmosphere, which extends to about 16.5 km elevation. In the default version of RegCM3, clouds are not permitted to form within the top two model layers, restricting clouds to a maximum elevation of about 14 km. However, the troposphere attains its maximum depth over the Maritime Continent and clouds are observed at altitudes up to 17 km, so it was considered appropriate to change the limitation on clouds to permit cloud formation within the second-top layer.

The model domain (Figure 1) was centered along the equator at 115^{o}E, used a normal Mercator projection, and spanned 95 grid points meridionally and 200 grid points zonally, with a horizontal resolution of 30 km. The simulations used 18 vertical sigma levels, from

the ground surface up to the 50 mb level. In all simulations presented, the land surface scheme was run every 120 seconds, twice the model time step.

Sea surface temperatures (SSTs) were prescribed using the National Ocean and Atmospheric Administration (NOAA) optimally interpolated SST (OISST) dataset, which is available at 1^{o} x 1^{o} resolution and at a weekly timescale (Reynolds *et al*. 2002). Topographic information was taken from the United States Geological Survey's Global 30 arc second elevation dataset (GTOPO30), aggregated to 10 arc minutes (United States Geological Survey 1996).

Vegetation biomes were based on the potential global vegetation dataset of Ramankutty (1999), modified to include two extra biomes for inland water and ocean as described in Winter *et al.* (2009). The vegetation biomes were used in conjunction with two additional datasets to populate each grid cell with plant functional types: 1) the monthly mean climatology of temperature (New *et al.* 1999), and 2) the minimum temperature ever recorded at a location minus the average temperature of the coldest month (Bartlein 2000). In all simulations presented, RegCM3-IBIS was run only with static vegetation.

Soil properties, such as albedo and porosity, were determined based on the relative proportions of clay and sand in each grid cell. Sand and clay percentages were taken from the Global Soil Dataset, which has a spatial resolution of 5 minutes (Global Soil Data Task, International Geosphere-Biosphere Programme, Data and Information System 2000). Soil moisture, soil temperature and soil ice content were initialized in RegCM3-IBIS using

the output from a global 0.5^{o} x 0.5^{o} resolution 20-year offline simulation of IBIS as described in Winter *et al.* (2009).

The European Centre for Medium-range Weather Forecasts (ECMWF) 40-year Re-Analysis (ERA40) dataset, available September 1957 to August 2002, (Uppala *et al.* 2005) was used to force the boundaries. The exponential relaxation technique of Davies and Turner (1977) was used at the boundaries.

Simulations were begun at 1 July 1997 and ended 31 December 2001. The first 6 months of output were ignored to allow for spin-up. The resulting four years of simulation (1998-2001) were used for evaluation of model performance. This time period was chosen for maximal overlap between the datasets used for lateral boundary conditions and the TRMM rainfall observational dataset used for comparison (described below).

A total of four simulations are presented in this study. Table 1 summarizes the different characteristics of these simulations and lists the names used to reference each simulation throughout the text.

d. Comparison Datasets

Several datasets are used for comparison to model output in this study.

To provide a sample of the mixed boundary layer over the Maritime Continent region, a new dataset was acquired from Changi Airport, Singapore. Ordinarily, radiosonde data are

collected at Changi Airport only twice per day – at 8 am and 8 pm local time (LT). However, greater temporal resolution was required for investigation of diurnal variation in the mixed boundary layer. Therefore additional radiosonde data were commissioned at 11 am and 2 pm LT during the period 1 October to 23 November 2010, when airport traffic allowed. (The regular 8 am and 8 pm soundings continued during this period.) In total, 35 soundings were acquired at 8 am LT, 28 soundings at 11 am LT, 29 soundings at 2 pm LT and 34 soundings at 8 pm LT. Temperature, relative humidity, dew point temperature, wind direction and wind speed measurements were recorded at 2 second intervals from the surface to a maximum elevation of 25-30 km, during an ascent that took 60-90 minutes.

It is noted that the Changi Airport data were collected over a limited time period, and some temporal variability in mixed boundary layer height may exist that is not captured by this sample. It is also acknowledged that these data represent a single point location and the mixed boundary layer height may vary spatially across the Maritime Continent. However, to the best of our knowledge, these data provide the only available estimate of mixed boundary layer height within this region, particularly at this high temporal resolution, and therefore provide an invaluable metric against which to assess the simulated height.

The radiosonde data were used to calculate vertical profiles of the potential temperature and water vapor mixing ratio. Figures 2 and 3 show, respectively, the vertical profiles of potential temperature and water vapor mixing ratio in the lowest 3 km of the atmosphere separated by the four times of day when measurements were made.

The mixed boundary layer height can be qualitatively estimated from these figures as the region of approximately constant potential temperature and water vapor mixing ratio, as shown in Table 2. Since potential temperature is a conserved quantity for all dry adiabatic processes, and the mixed boundary layer is approximately adiabatic, potential temperature should remain approximately constant throughout that depth. In addition, water vapor should be well-mixed over the same depth. A similar method for estimating the mixed boundary layer using temperature and mixing ratio profiles during daytime (unstable) conditions was used by Joffre *et al.* (2001).

To provide a more quantitative estimate, the mixed boundary layer height was calculated as the elevation at which the vertical gradient of potential temperature ($\Delta\theta / \Delta z$) exceeded 0.005 K m^{-1}, in accordance with condition 1 of Heffter (1980). To remove noise in the radiosonde data due to the 2-second sampling interval, a moving-average window of 100 m depth was calculated before estimating the vertical gradient of potential temperature. Table 3 shows statistics of the mixed boundary layer height calculated using this method from all the radiosonde profiles shown in Figures 2 and 3. Note that, due to the size of the averaging window, the minimum height returned with this algorithm is 90 m.

The actual mixed boundary layer height over Singapore is likely to be somewhere between these qualitative and quantitative estimates. Hence the mixed boundary layer height used for comparison to the model output was taken to be 250 m at 8 am, 800 m at 11 am, 750 m at 2 pm and 500 m at 8 pm.

The estimated height at 8 am from the Changi Airport data is consistent with measurements made of the nocturnal and early morning PBL height over sub-tropical and mid-latitude locations. Benkley and Schulman (1979) showed that the early morning PBL height was about 330 m over a smooth, flat Illinois site. Koracin and Berkowicz (1988) showed that the nocturnal PBL height was approximately 180 m over central Illinois, using data obtained through the Electric Power Research Institute (EPRI) Plume Model Validation and Development (PMVD) Project. Tombrou *et al*. (1998) presented rawinsonde data that showed a mean nocturnal PBL height of about 350 m over Helliniko airport near Athens, Greece. Contini *et al*. (2008) showed that the nocturnal PBL height was about 300 m based on data collected from a meteorological station in Lecce, Italy. Similar measurements published for tropical locations were not found for comparison to the Changi Airport data.

Comparison between simulated and observed boundary layer height must consider that a meteorological station represents a point-scale measurement, while a model grid cell represents the average condition over a much larger area. The resolution of the model domain used here results in loss of some of the smaller islands, and Singapore is approximated as the southern-most grid cell of the simulated Peninsula. But the meteorological station at Changi Airport is located at the eastern edge of the island, and will sample air that represents a mix of land- and ocean-derived conditions. For example, if wind is recorded in a southerly or easterly direction at Changi Airport, the sounding will measure conditions originating from the ocean, while winds recorded from the north or west will measure conditions more typical of the land.

Table 4 shows the mean wind speed and direction measured by the Changi Airport radiosonde for each time of day that was sampled in the new dataset, averaged over different depths starting at the surface (i.e. the depths represent the lowest X m of the atmosphere). The estimated PBL height is shown for comparison. A wind direction of 0 degrees signifies wind coming from the north; direction is calculated clockwise from north.

Table 4 shows that there is little diurnal variability in either wind direction or wind speed when averaged over the lowest 1000 m. As the averaging depth is made shallower and brought closer to the surface, the wind directions and speeds exhibit increasing diurnal variability. At lower elevations, the early morning winds are westerly but weaker, while the afternoon winds are more southerly and stronger. This pattern is consistent with a land-sea breeze circulation, which is known to be a strong feature in this region.

Therefore the wind data suggest that a land grid cell from the model is likely the most appropriate comparison to the observations at 8 am LT. But throughout the rest of the day, either an ocean grid cell or an average of land and ocean grid cells should provide the most appropriate comparison. Hence both land and ocean grid cells from the model domain will be used for comparison to the Changi Airport data.

The horizontal extent of cloud cover simulated by the model was compared to the International Satellite Cloud Climatology Project (ISCCP) Stage D2 product (Rossow *et al.* 1996), made available by NASA. This provides the fractional cloud cover at three

elevations: high (50-440 mb), middle (440-680 mb) and low (680-1000 mb), at 280 km resolution and monthly timescales. Data was averaged over the period 1998-2001 to compare to the model. Model output was aggregated to the same horizontal grid as the ISCCP data. To match up the vertical resolution, the model output was aggregated in the vertical assuming random overlap of clouds between layers, using layers 2-8 (roughly 760-1000 mb) for the low clouds, layers 9-12 (roughly 450-700 mb) for the middle clouds, and 13-17 (roughly 100-400 mb) for the high clouds.

Solar radiation is compared to the NASA/GEWEX (Global Energy and Water Cycle Experiment)'s Surface Radiation Budget (SRB) dataset Release 3.0 (Stackhouse *et al.* 2011), made available by the NASA Langley Research Center Atmospheric Sciences Data Center. This dataset is available at 3-hourly intervals on a 1^{o} x 1^{o} global grid. The data was interpolated to the model domain for direct comparison to simulation output.

Observations of latent heat flux over land are taken from direct observations of evapotranspiration (ET) in the Maritime Continent region, as described in Table 4 of Gianotti *et al.* (2012). Over ocean, latent and sensible heat flux observations are from the Woods Hole Oceanographic Institute (WHOI) Global Dataset of Ocean Evaporation (Yu *et al.* 2008). The WHOI observations compare well with data collected during the TOGA COARE experiment (Webster *et al.* 1996, Weller and Anderson 1996, Lau and Sui 1997, Sui *et al.* 1997, Emanuel and Živković-Rothman 1999).

Total rainfall is compared to data from the Tropical Rainfall Measuring Mission (TRMM) Multisatellite Precipitation Analysis (TMPA) 0.25^{o} x 0.25^{o} 3B42 product (described in Huffman *et al.* 2007), referenced in this work simply as TRMM. TRMM is available from January 1998 to the present day, and is one of the highest resolution datasets available over the Maritime Continent. Relative proportions of convective and large-scale rain are taken from Mori *et al.* (2004), who used the 2A25, 2A12 and 2B31 TRMM products to describe the climatological convective versus stratiform rainfall split over Indonesia.

3. Results and Discussion

a. Planetary Boundary Layer Height

Figure 4 compares the estimated PBL height from the Changi Airport soundings to simulated values from the default version of RegCM3-IBIS using both the Grell with Fritsch-Chappell closure and Emanuel convection schemes (model output is averaged over the period 1998-2001). The figure shows the PBL height simulated for a land grid cell, at the approximate location of Singapore at the southern end of the Malay Peninsula, and for the ocean grid cell immediately adjacent. The average value for the PBL height at each time of day is denoted by the star markers for the Changi data and by the dashed lines for the model output. The vertical bars indicate the observed and simulated variability of the PBL height at each time of day, and are calculated using the unbiased estimator for the standard deviation.

Figure 4 indicates that the simulated PBL height over the land grid cell nearest to Singapore is substantially higher than the height estimated from the Changi Airport

soundings. It was suggested previously that the land grid cell should be the most appropriate comparison to the observations in the early morning, when winds are light and westerly. However, the simulated early morning PBL height over land is about 800 m higher than observations, indicating that the simulated PBL in the default version of RegCM3 does not collapse appropriately at night. During the daytime, Figure 4 indicates that the simulated PBL over the nearby ocean is substantially lower than over land and is a much closer match to the observations.

Figure 5 shows the average diurnal cycle of the PBL height simulated using the modified PBL scheme within RegCM3, comparing a land grid cell to an ocean grid cell as the approximate location of Singapore as described above. The estimated PBL height from the Changi radiosonde data is shown for comparison. Table 5 summarizes the approximate height of the simulated PBL at the times corresponding to the Changi radiosonde data using the modified version of RegCM3-IBIS.

The results show that the modifications made to the PBL scheme significantly improve the simulated PBL height over Singapore. The new PBL scheme captures the low PBL height that is shown in the observations in the morning and evening, which was significantly overestimated in the default scheme. If a land grid cell is an appropriate comparison to the Changi sounding data in the early morning and evening, and an ocean grid cell is the appropriate comparison during the daytime as discussed earlier, then the Emanuel scheme in particular provides a good match to the observed PBL height. These results indicate that the modified PBL scheme results in a much more physically-realistic PBL simulation over

Singapore. Therefore is considered that the modified PBL scheme will better represent the diurnal evolution of the PBL height over the Maritime Continent compared to the default scheme.

b. Low-level Cloud Cover

Figures 6 and 7 show, respectively, the diurnal cycle of cloud fraction simulated by the default and modified versions of RegCM3-IBIS using the Emanuel convection scheme. Cloud fraction simulated using the Grell with Fritsch-Chappell closure convection scheme was qualitatively similar and therefore is not shown here for brevity.

The figures show that the new representation of PBL clouds significantly reduces the low-level cloud cover in the modified version of the model, particularly over land grid cells, at all times of the day. The impact is particularly noticeable at night, when the greatest fractional cloud cover is simulated in the default version of the model.

Over ocean grid cells, the default version of the model simulates a thin layer of clouds at approximately 500 m elevation, similar to the marine boundary layer clouds commonly observed and consistent with the cloud base shown for the Pacific Ocean by Wang *et al.* (2004). Therefore the impact of changing the representation of PBL clouds is less significant over the ocean grid cells in the modified version of the model.

Figure 8 shows the difference in low-level cloud cover between the ISCCP data and the simulated results from the default and modified versions of the model, using both the Grell

with Fristch-Chappell closure and Emanuel convection schemes. Both the ISCCP data and model output are averaged over the period 1998-2001.

Figure 8 shows that the modified version of the model, with both the Grell Fritsch-Chappell and Emanuel convection schemes, reduces the simulated overestimation bias in low-level cloud cover, bringing the simulation results closer to the observations. The impact is particularly noticeable over land grid cells, indicating that the reduction in night-time low-level clouds shown in Figure 7 brings the simulation results closer to reality.

c. Radiative and Turbulent Heat Fluxes

Table 6 shows the average daily fluxes of shortwave and net radiation and turbulent heat with respect to the surface, averaged separately for land and ocean grid cells over the period 1998-2001. Observations from SRB are compared to the default and modified versions of the model using both convection schemes.

Table 6 shows that incoming and net absorbed solar radiation are overestimated in both the default and modified versions of the model. The modifications made to simulation of the PBL region worsened the overestimation bias present in the default version of the model due to the removal of low-level cloud cover. Although there was an increase in very high cloud cover, which was due to the modified limitation on high clouds, it was not sufficient to offset the reduction in low-level cloud cover over land. Over ocean, the overestimation bias in solar radiation was reduced slightly due to the increase in high cloud cover, since there was little change in the simulated low-level cloud cover over ocean. These errors in

solar radiation exist despite good simulation of the planetary albedo, and are the subject of concurrent work on convective cloud cover by these authors (Gianotti and Eltahir, *manuscript submitted to J. Climate*).

The simulated errors in solar radiation propagate into overestimation bias in net radiation at the surface, which in turn translates into overestimation of turbulent heat fluxes. The errors are different between the convection schemes due to differences in the simulated rainfall: the Grell scheme simulates less rainfall and therefore a drier surface, resulting in overestimation of sensible heat flux, while the Emanuel scheme simulates more rainfall and a wetter surface, resulting in overestimation of latent heat flux. Similar errors were documented in the default version of the model in Gianotti *et al.* (2012).

d. Rainfall

Table 7 shows the daily rainfall averaged over the period 1998-2001 separately for land and ocean, including the relative convective and large-scale rainfall fractions. These results illustrate the response of the system to the changes in radiative and turbulent heat fluxes resulting from the modifications to the PBL region, which had opposite effects on convection.

Reduction of the simulated PBL height reduced the convective rainfall because the shallower mixed region limited the ability of moist air parcels to be lifted to a level of saturation (i.e. the lifted condensation level). This effect is evident in the modified simulation using the Emanuel convection scheme. On the other hand, reduction of the low-

level cloud cover led to increased net radiation at the surface and therefore increased low-level instability, driving greater convective mass flux and more convective rainfall. This effect is evident in the simulation using the Grell scheme with Fritsch-Chappell closure.

The large-scale rainfall volume increased with both convection schemes primarily due to the increase in high cloud cover created by the altered limitation on clouds within the second-top model layer. The high clouds are almost entirely large-scale in nature. Rainfall simulated by the SUBEX routine is strongly dependent on the fractional coverage of large-scale clouds and therefore the increase in large-scale rainfall is a direct result of this increase in high clouds.

With both convection schemes, the modifications to the mixed boundary layer improved the simulation of convective rainfall volume over both land and ocean – increasing it with the Grell scheme and reducing it with the Emanuel scheme, bringing both simulations closer to the TRMM observations. However, the modifications also led to significant increases in large-scale rainfall with both schemes compared to the default model, which produced an overestimation bias and worsened the total rainfall compared to TRMM. These errors in rainfall are explored further in concurrent work by these authors (Gianotti and Eltahir, *manuscript submitted to J. Climate*).

4. Summary

This paper has shown that the default version of RegCM3-IBIS exhibits significant error in the simulation of quantities that stimulate convective motion, including the height of the

mixed boundary layer, low-level cloud cover and incoming solar radiation. Modifications were made to improve the simulation of the mixed boundary layer by: reducing the mixed boundary layer height, particularly at night-time, by updating the Holtslag parameterization scheme and removing an inappropriate description of the nocturnal boundary layer height; and limiting representations of large-scale clouds within the mixed boundary layer until the entire depth reaches bulk saturation.

The work presented here shows that these changes significantly affected the simulation of both convective and large-scale rainfall. The modifications made here had positive impacts on the simulation of convective rainfall within RegCM3-IBIS when using both the Grell and Emanuel convection schemes.

However, the modifications were not sufficient to address the simulation errors that were identified in Gianotti *et al.* (2012), and actually worsened the existing overestimation bias in solar and net radiation at the surface while producing a significant overestimation bias in large-scale rainfall over land. Therefore this work indicates that 1) accurate simulation of the PBL region is essential but not sufficient for achieving good simulation of rainfall over the Maritime Continent region, and 2) there is another significant source of error in the simulation of rainfall within RegCM3-IBIS.

This work was motivated by the work of Gianotti *et al.* (2012), which indicated that the primary source of error in RegCM3 resided in the simulation of convective rainfall. Moist convection both responds to and influences conditions within the PBL region. While this

paper has investigated the simulation of surface fluxes and growth of the mixed boundary layer, which influence the initiation of convection, it remains to investigate the feedback of moist convection on the near surface environment. The impact of convective activity on the surface via cumulus cloud and rainfall production is the subject of concurrent work by these authors (Gianotti and Eltahir, *manuscript submitted to J .Climate*), which addresses the errors in rainfall production documented here.

Acknowledgements

Funding for this study was provided by the Singapore National Research Foundation through the Singapore-MIT Alliance for Research and Technology (SMART) Center for Environmental Sensing and Modeling (CENSAM). RLG was also supported by the MIT Martin Family Society of Fellows for Sustainability. Meteorological data measured at Changi Airport in Singapore was provided by the National Environment Agency of Singapore. The authors thank an anonymous reviewer for comments that helped to improve the manuscript.

References

Albrecht, B. A., C. S. Bretherton, D. W. Johnson, W. H. Schubert, and A. S. Frisch, 1995: The Atlantic Stratocumulus Transition Experiment – ASTEX, *Bull. Am. Meteorol. Soc.*, **76**, 889-904.

Albrecht, B. A., D. A. Randall, and S. Nicholls, 1988: Observations of marine stratocumulus during FIRE, *Bull. Am. Meteorol. Soc*., **69**, 618-626.

Anthes, R. A, 1977: A cumulus parameterization scheme utilizing a one-dimensional cloud model, *Mon. Weather Rev.*, **105**, 270-286.

Bachiochi, D. R., and T. N. Krishnamurti, 2000: Enhanced low-level stratus in the FSU coupled ocean-atmosphere model, *Mon. Weather Rev*., **128**, 3083-3103.

Bartlein, P., 2000: *Absolute minimum temperature minus average of the coldest monthly mean temperature Worldwide Airfield Summaries* [Available online at: http://www.sage.wisc.edu/download/IBIS].

Benkley, C. W., and L. L. Schulman, 1979: Estimating hourly mixing depths from historical meteorological data, *J. Appl. Meteorol*., **18**, 772-780.

Bony, S., and J.-L. Dufresne, 2005: Marine boundary layer clouds at the heart of tropical cloud feedback uncertainties in climate models, *Geophys. Res. Letters*, **32**, L20806, doi:10.1029/2005GL023851.

Bretherton, C. S., and Coauthors, 2004: The EPIC 2001 stratocumulus study, *Bull. Am. Meteorol. Soc.*, **85**, 967-977.

Bretherton, C. S., and Coauthors, 1999: A GCSS boundary-layer cloud model intercomparison study of the first ASTEX Lagrangian experiment, *Boundary-Layer Meteorol.*, **93**, 341–380.

Cha, D.-H., D.-K. Lee, and S.-Y. Hong, 2008: Impact of boundary layer processes on seasonal simulation of the East Asian summer monsoon using a Regional Climate Model, *Meteorol. Atmos. Phys.*, **100**, pp. 53-72.

Christensen, J. H., B. Hewitson, A. Busuioc *et al.*, 2007: Regional Climate Projections, In *Climate Change 2007: The Physical Science Basis. Contribution of Working Group I to the Fourth Assessment Report of the Intergovernmental Panel on Climate Change* [Solomon, S., D. Qin, M. Manning, Z. Chen, M. Marquis, K. B. Averyt, M. Tignor, and H. L. Miller (eds.)]. Cambridge University Press, Cambridge, United Kingdom, and New York, NY, USA.

Contini, D., D. Cava, P. Martano, A. Donateo, and F. M. Grasso, 2008: Boundary layer height estimation by sodar and sonic anemometer measurements, *IOP Conf. Ser.: Earth Environ. Sci.*, **1**, doi:10.1088/1755-1307/1/1/012034.

Dai, A., and K. E. Trenberth, 2004: The diurnal cycle and its depiction in the Community Climate System Model, *J. Clim.*, **17**, 930-951.

Davies, H., and R. Turner, 1977: Updating prediction models by dynamical relaxation: An examination of the technique, *Q. J. R. Meteorol. Soc.*, **103**, 225-245.

de Vries, D. A., 1963: Chapter 7: Thermal properties of soils, in *Physics of Plant Environment*, W. R. van Wijk (Ed.), North-Holland Publishing Company, 210-235.

Dickinson, R., A. Henderson-Sellers, and P. Kennedy, 1993: Biosphere Atmosphere Transfer Scheme (BATS) version 1e as coupled to the NCAR Community Climate Model, *NCAR Technical Note NCAR/TN-387+STR*, National Center for Atmospheric Research, Boulder, Colorado.

Emanuel, K. A., 1991: A scheme for representing cumulus convection in large-scale models, *J. Atmos. Sci.*, **48**(21), 2313-2335.

Emanuel, K. A., and M. Zivkovic-Rothman, 1999: Development and evaluation of a convection scheme for use in climate models, *J. Atmos. Sci.*, **56**, 1766-1782.

Fairall, C. W., E. F. Bradley, J. E. Hare, A. A. Grachev and J. B. Edson, 2003: Bulk parameterization of air-sea fluxes: updates and verification for the COARE algorithm, *J. Clim*., **16**, 571-591.

Fairall, C. W., E. F. Bradley, D. P. Rogers, J. B. Edson and G. S. Young, 1996: Bulk parameterization of air-sea fluxes for Tropical Ocean-Global Atmosphere Coupled-Ocean Atmosphere Response Experiment, *J. Geophys. Res*., **101**(C2), 3747-3764.

Farouki, O. T., 1981: The thermal properties of soils in cold regions, *Cold Regions Science and Technology*, **5**, 67-75.

Foley, J. A., I. C. Prentice, N. Ramankutty, S. Levis, D. Pollard, S. Sitch, and A. Haxeltine, 1996: An integrated biosphere model of land surface processes, terrestrial carbon balance, and vegetation dynamics, *Global Biogeochem. Cycles*, **10**(4), 603-628.

Frey, H., M. Latif, and T. Stockdale, 1997: The coupled GCM ECHO-2. Part I: The tropical Pacific, *Mon. Weather Rev*., **125**, 703-720.

Fritsch, J. M., and C. F. Chappell, 1980: Numerical prediction of convectively driven mesoscale pressure systems. Part 1: Convective parameterization, *J. Atmos. Sci.*, **37**, 1722-1733.

Gianotti, R. L., and E. A. B. Eltahir, Regional climate modeling over the Maritime Continent. Part II: New parameterization for autoconversion of convective rainfall, *J. Climate*, manuscript submitted.

Gianotti, R. L., D. Zhang, and E. A. B. Eltahir, 2012: Assessment of the Regional Climate Model Version 3 over the Maritime Continent using different cumulus parameterization and land surface schemes, *J. Clim*., **25**, 638-656.

Gianotti, R. L., 2012: *Convective cloud and rainfall processes over the Maritime Continent: Simulation and analysis of the diurnal cycle*, PhD Dissertation, Massachusetts Institute of Technology, Cambridge, MA.

Giorgi, F., E. Coppola, F. Solomon and Coauthors, 2012: RegCM4: model description and preliminary tests over multiple CORDEX domains, *Clim. Res.*, **52**, 7-29.

Global Soil Data Task, International Geosphere-Biosphere Programme, Data and Information System, 2000: *Global soil data products CD-ROM*, International Geosphere-Biosphere Programme, Data and Information System (IGDP-DIS), Potsdam, Germany.

Grell, G. A., 1993: Prognostic evaluation of assumptions used by cumulus parameterizations, *Mon. Weather Rev.*, **121**, 764-787.

Grell, G. A., J. Dudhia, and D. R. Stauffer, 1994: Description of the fifth generation Penn State/NCAR Mesoscale Model (MM5), *Technical Report TN-398+STR*, National Center for Atmospheric Research, Boulder, Colorado.

Heffter, J. L., 1980: Transport layer depth calculations, *Second Joint Conference on Applications of Air Pollution Meteorology*, New Orleans, USA.

Holtslag, A. A. M., and B. A. Boville, 1993: Local versus nonlocal boundary-layer diffusion in a global climate model, *J. Clim*., **6**, 1825-1842.

Holtslag, A. A. M., E. I. F. de Bruijn, and H.-L. Pan, 1990: A high-resolution air mass transformation model for short-range weather forecasting, *Mon. Weather Rev.*, **118**, 1561-1575.

Huffman, G. J., R. F. Adler, D. T. Bolvin, G. Gu, E. J. Nelkin, K. P. Bowman, Y. Hong, E. F. Stocker, and D. B. Wolff, 2007: The TRMM Multisatellite Precipitation Analysis (TMPA): Quasi-Global, Multiyear, Combined-Sensor Precipitation Estimates at Fine Scales, *J. Hydrometeorol.*, **8**, 38-55.

Joffre, S. M., M. Kangas, M. Heikinheimo, and S. A. Kitaigorodskii, 2001: Variability of the stable and unstable atmospheric boundary-layer height and its scales over a boreal forest, *Boundary-Layer Meteorol.*, **99**, 429-450.

Karlsson, J., G. Svensson, S. Cardoso, J. Teixeira and S. Paradise, 2010: Subtropical cloud-regime transitions: Boundary layer depth and cloud-top height evolution in models and observations, *J. App. Meteorol. Clim.*, **49**, 1845-1858.

Kiehl, J. T., J. J. Hack, G. B. Bonan, B. A. Boville, B. P. Breigleb, D. L. Williamson, and P. J. Rasch, 1996: Description of the NCAR Community Climate Model (CCM3), *NCAR Technical Note TN-420+STR*, [Available online at: http://www.cgd.ucar.edu/cms/ccm3/TN-420/].

Koracin, D., and R. Berkowicz, 1988: Nocturnal boundary-layer height: observations made by acoustic sounders and predictions in terms of surface layer parameters, *Bound.-Layer Meteorol.*, **43**, 65-83.

Krueger, S. K., G. T. McLean, and Q. Fu, 1995: Numerical simulation of the stratus-to-cumulus transition in the subtropical marine boundary layer. Part I: Boundary-layer structure, *J. Atmos. Sci*., **52**, 2839–2850.

Lau, K.-M., and C.-H. Sui, 1997: Mechanisms of short-term sea surface temperature regulation: Observations during TOGA COARE, *J. Clim*., **10**, 465-472.

Lin, W. Y., and M. H. Zhang, 2004: Evaluation of clouds and their radiative effects simulated by the NCAR Community Atmospheric Model against satellite observations, *J. Clim.*, **17**, 3302-3318.

Martin, G. M., M. R. Bush, A. R. Brown, A. P. Lock, and R. N. B. Smith, 2000: A new boundary layer mixing scheme. Part II: Tests in climate and mesoscale models, *Mon. Weather Rev*., **128**, 3200-3217.

McCaa, J. R., and C. S. Bretherton, 2004: A new parameterization for shallow cumulus convection and its application to marine subtropical cloud-topped boundary layers. Part II: Regional simulations of marine boundary layer clouds, *Mon. Weather Rev.*, **132**, 883-896.

Mori, S., H. Jun-Ichi, Y. I. Tauhid, M. D. Yamanaka, N. Okamoto, F. Murata, N. Sakurai, H. Hashiguchi, and T. Sribimawati, 2004: Diurnal land-sea rainfall peak migration over

Sumatera Island, Indonesian Maritime Continent, observed by TRMM satellite and intensive rawinsonde soundings, *Mon. Weather Rev.*, **132**, 2021-2039.

Neale, R. B., J. H. Richter, A. J. Conley, S. Park, P. H. Lauritzen, A. Gettelman, D. L. Williamson, P. J. Rasch, S. J. Vavrus, M. A. Taylor, W. D. Collins, M. Zhang, and S.-J. Lin, 2010: Description of the NCAR Community Atmosphere Model (CAM 4.0), *Technical Note NCAR/TN-485+STR*, National Center for Atmospheric Research, Boulder, Colorado.

Neale, R., and J. Slingo, 2003: The Maritime Continent and its role in the global climate: A GCM study, *J. Clim.*, **16**, 834-848.

New, M., M. Hulme, and P. Jones, 1999: Representing twentieth-century space-time climate variability. Part I: Development of a 1961-90 mean monthly terrestrial climatology, *J. Clim.*, **12**, 829-856.

Pal, J. S., and Coauthors, 2007: Regional climate modeling for the developing world: The ICTP RegCM3 and RegCNET, *Bull. Am. Meteorol. Soc.*, **88**, 1395-1409.

Pal, J. S., E. E. Small, and E. A. B. Eltahir, 2000: Simulation of regional-scale water and energy budgets: Representation of subgrid cloud and precipitation processes within RegCM, *J. Geophys. Res. [Atmos.]*, **105(D24)**, 579-594.

Ramankutty, N., 1999: Estimating historical changes in land cover: North American croplands from 1850 to 1992, *Global Ecol. Biogeogr.*, **8**, 381-396.

Rauber, R. M., and Coauthors, 2007: Rain in Shallow Cumulus over the Ocean: The RICO campaign, *Bull. Am. Meteorol. Soc.*, **88**, 1912–1928.

Reynolds, R. W., N. Rayner, T. Smith, D. Stokes, and W. Wang, 2002: An improved in situ and satellite SST analysis for climate, *J. Clim.*, **15**, 1609-1625.

Rossow, W. B., A. W. Walker, D. E. Beuschel, and M. D. Roiter, 1996: *International Satellite Cloud Climatology Project (ISCCP) Documentation of New Cloud Datasets*, WMO/TD-No. 737, World Meteorological Organization, 115 pp.

Seidel, D. J., Y. Zhang, A. Beljaars, J.-C. Golaz, A. R. Jacobson, and B. Medeiros, 2012: Climatology of the planetary boundary layer over the continental United States and Europe, *J. Geophys. Res*., **117**, D17106, doi:10.1029/2012JD018143.

Smith, R. N. B., 1990: A scheme for predicting layer clouds and their water content in a general circulation model, *Q. J. R. Meteorol. Soc.*, **116**, 435-460.

Stackhouse, Jr., P. W., S. K. Gupta, S. J. Cox, J. C. Mikovitz, T. Zhang, and L. M. Hinkelman, 2011: The NASA/GEWEX Surface Radiation Budget Release 3.0: 24.5-Year Dataset, GEWEX News, 21(1), February, 10-12.

Stevens, B., and Coauthors, 2003: Dynamics and Chemistry of Marine Stratocumulus—DYCOMS-II, *Bull. Am. Meteorol. Soc.*, **84**, 579–593.

Stull, R. B, 1988: *An Introduction to Boundary Layer Meteorology*, Kluwer Academic Publishers, 666 p.

Sui, C.-H., X. Li, K.-M. Lau, and D. Adamec, 1997: Multiscale air-sea interactions during TOGA COARE, *Mon. Weather Rev.*, **125**, 448-462.

Sun, L., F. H. M. Semazzi, F. Giorgi and L. Ogallo, 1999: Application of the NCAR regional climate model to eastern Africa. 1. Simulation of the short rains of 1988, *J. Geophys. Res.*, **104**(D6), 6529-6548.

Sundqvist, H., 1988: Parameterization of condensation and associated clouds in models for weather prediction and general circulation simulation, in *Physically-based Modelling and Simulation of Climate and Climatic Change*, M. E. Schlesinger (Ed.), Reidel, 433-461.

Svensson, G., M. Tjernström and D. Koracin, 2000: The sensitivity of a stratocumulus transition: Model simulations of the ASTEX first Lagrangian, *Boundary-Layer Meteorol.*, **95**, 57–90.

Tombrou, M., D. Founda, and D. Boucouvala, 1998: Nocturnal boundary layer height prediction from surface routine meteorological data, *Meteorol. Atmos. Phys*., **68**, 177-186.

United States Geological Survey, 1996: *Global 30-arc second elevation dataset (GTOPO30)*, [Available online at: http://eros.usgs.gov/#/Find_Data/Products_and_Data_Available/gtopo30_info].

Uppala, S. M., and Coauthors, 2005: The ERA-40 Re-Analysis, *Q. J. R. Meteorol. Soc.*, **131**, 2961-3012. [Dataset available online at: http://www.ecmwf.int/research/era/do/get/era-40].

Verseghy, D. L., 1991: Class-A Canadian land surface scheme for GCMS. I. Soil model, *Int. J. Clim.*, **11**, 111-133.

Vogelezang, D. H. P., and A. A. M. Holtslag, 1996: Evaluation and model impacts of alternative boundary-layer height formulations, *Boundary-Layer Meteorol.*, **81**, 245-269.

Wang, Y., L. Zhou, and K. Hamilton, 2007: Effect of convective entrainment / detrainment on the simulation of the tropical precipitation diurnal cycle, *Mon. Weather Rev.*, **135**, 567-585.

Wang, Y., S.-P. Xie, H. Xu, and B. Wang, 2004: Regional model simulations of marine boundary layer clouds over the South Pacific off South America. Part I: Control experiment, *Mon. Weather Rev*., **132**, 274-296.

Webster, P. J., C. A. Clayson, and J. A. Curry, 1996: Clouds, radiation, and the diurnal cycle of sea surface temperature in the tropical western Pacific, *J. Clim*., **9**, 1712-1730.

Weller, R. A., and S. P. Anderson, 1996: Surface meteorology and air-sea fluxes in the western equatorial Pacific warm pool during the TOGA coupled ocean-atmosphere response experiment, *J. Clim*., **9**, 1959-1990.

Winter, J. M., J. S. Pal, and E. A. B. Eltahir, 2009: Coupling of Integrated Biosphere Simulator to Regional Climate Model Version 3, *J. Clim.*, **22**, 2743-2757.

Yang, G.-Y., and J. Slingo. 2001: The diurnal cycle in the tropics, *Mon. Weather Rev.*, **129**, 784-801.

Yu, L., X. Jin, and R. A. Weller, 2008: Multidecade global flux datasets from the objectively analyzed air-sea fluxes (OAFlux) project: Latent and sensible heat fluxes,

ocean evaporation, and related surface meteorological variables, *Woods Hole Oceanographic Institution OAFlux Project Technical Report (OA-2008-01)*, [Available online at: http://oaflux.whoi.edu/pdfs/OAFlux_TechReport_3rd_release.pdf].

Yu, T. W., 1978: Determining the height of the nocturnal boundary layer, *J. Appl. Meteorol*., **17**, 481-485.

Zeng, X., M. Zhao, and R. E. Dickinson, 1998: Intercomparison of bulk aerodynamic algorithms for the computation of sea surface fluxes using TOGA COARE and TAO data, *J. Clim.*, **11**, 2628-2644.

Zilitinkevich, S., and A. Baklanov, 2002: Calculation of the height of the stable boundary layer in practical applications, *Boundary-Layer Meteorol.*, **105**, 389-409.

Table 1. Varying characteristics of simulations used in study. The names are used to reference each simulation in the text.

Simulation Name	Convection Scheme	PBL Region*
GFC-Def	Grell with F-C	Default
GFC-Mod	Grell with F-C	Modified
EMAN-Def	Emanuel	Default
EMAN-Mod	Emanuel	Modified

* Refers to simulation of mixed boundary layer height, Zeng ocean flux scheme, soil heat flux and non-convective clouds within the mixed boundary layer

Table 2. Mixed boundary layer height (in m) over Changi airport estimated qualitatively from radiosonde data using depth of constant potential temperature (theta) and water vapor mixing ratio, as shown in Figures 2 and 3.

Height (m)	8 am LT	11 am LT	2 pm LT	8 pm LT
Constant mixing ratio	300	600	700	300
Constant potential temperature	0	900	900	200

Table 3. Characteristics of mixed boundary layer height (in m) over Changi Airport estimated from radiosonde data using threshold of vertical gradient in potential temperature, in accordance with condition 1 of Heffter (1980).

Height (m)	8 am LT	11 am LT	2 pm LT	8 pm LT
Mean	225	811	731	676
Maximum	810	1340	1540	1750
Minimum	90	90	90	90
Standard deviation	201	295	464	503

Table 4. Mean wind speed (in m s^{-1}) and direction (in deg) measured by Changi airport radiosonde data.

	8 am LT		11 am LT		2 pm LT		8 pm LT	
PBL height	250 m		800 m		750 m		500 m	
Averaging Depth	Direction (deg)	Speed (m s^{-1})	Direction (deg)	Speed (m s^{-1})	Direction (deg)	Speed (m s^{-1})	Direction (deg)	Speed (m s^{-1})
1000 m	251	4.9	251	4.2	244	4.6	251	4.0
500 m	260	3.8	246	3.6	237	4.2	243	3.3
250 m	295	2.8	242	3.2	233	4.0	243	2.9
100 m	313	1.8	241	2.7	229	3.4	246	2.3

Table 5. Mixed boundary layer height (in m) comparison between the Changi sounding data estimate and values simulated using the modified version of RegCM3-IBIS, using land and ocean model grid cells close to the location of Singapore.

Simulation	8 am LT	11 am LT	2 pm LT	8 pm LT
Changi radiosonde	*250 m*	*800 m*	*750 m*	*500 m*
GFC-Mod land cell	382	990	1375	800
GFC-Mod ocean cell	674	708	704	655
EMAN-Mod land cell	249	959	1180	456
EMAN-Mod ocean cell	680	726	754	758

Table 6. Average daily surface radiation and turbulent heat fluxes over period 1998-2001 for (upper) land and (lower) ocean grid cells within the domain, from simulations using the default ('-Def') and modified ('-Mod') versions of the model. All radiative and turbulent fluxes are in units of W m^{-2}.

Product / Simulation	SW_{dn}	SW_{net}	Planetary albedo	R_N	LH	SH
Observations	*202*	*171*	*48%*	*129*	*95*	*34*
GFC-Def	225	194	45%	141	104	36
GFC-Mod	257	222	44%	164	118	48
EMAN-Def	213	183	50%	141	134	6
EMAN-Mod	237	204	49%	157	137	21

Product / Simulation	SW_{dn}	SW_{net}	Planetary albedo	R_N	LH	SH
Observations	*220*	*206*	*45%*	*158*	*108*	*10*
GFC-Def	264	247	40%	188	129	12
GFC-Mod	261	245	43%	184	128	15
EMAN-Def	257	241	45%	186	126	4
EMAN-Mod	251	235	49%	182	118	7

Notes on table: SW_{dn} = shortwave (solar) radiation incident at the surface, SW_{net} = net absorbed shortwave radiation at the surface, R_N = net radiation absorbed at the surface, LH = latent heat flux away from the surface, SH = sensible heat flux away from the surface.

Table 7. Average daily rainfall over land and ocean over period 1998-2001 for simulations with default and modified model. All values are in units of mm day^{-1}.

Product / Simulation	Land Average			Ocean Average		
	Total	Convective	Large-scale	Total	Convective	Large-scale
TRMM	*8.7*	*5.5 (63%)*	*3.2 (37%)*	*7.0*	*4.0 (57%)*	*3.0 (43%)*
GFC-Def	8.5	3.7 (43%)	4.8 (57%)	6.7	3.8 (56%)	2.9 (44%)
GFC-Mod	10.9	4.4 (40%)	6.5 (60%)	8.5	4.1 (48%)	4.4 (52%)
EMAN-Def	14.9	11.9 (80%)	3.0 (20%)	7.2	6.2 (86%)	1.0 (14%)
EMAN-Mod	16.8	9.9 (59%)	6.9 (41%)	6.7	3.8 (57%)	2.9 (43%)

Fig. 1 Model domain showing vegetation classification used for IBIS. The domain has been sized such that it covers the generally accepted extent of the Maritime Continent region. Major islands are labeled

Fig. 2 Profiles of potential temperature for lowest 3 km of atmosphere from Changi Airport radiosonde data, 1 October – 23 November 2010. (a) 8 am LT; (b) 11 am LT; (c) 2 pm LT; (d) 8 pm LT. Grey lines show individual soundings; black line shows mean profile

Fig. 3 Profiles of water vapor mixing ratio for lowest 3 km of atmosphere from Changi Airport radiosonde data, 1 October – 23 November 2010. (a) 8 am LT; (b) 11 am LT; (c) 2 pm LT; (d) 8 pm LT. Grey lines show individual soundings; black line shows mean profile

Fig. 4 Diurnal PBL height (in m) over or near Singapore, simulated by the default version of RegCM3-IBIS using (top) Grell Fritsch-Chappell and (bottom) Emanuel convection schemes using either a land (blue) or ocean (green) grid cell to represent Singapore, compared to the PBL height estimated from the Changi soundings (black stars; dotted lines are shown to interpolate between the measurement times). The vertical bars signify one standard deviation of each sample set and illustrate the variability in the simulated and observed PBL height

Fig. 5 As in Figure 4 but for the modified version of RegCM3-IBIS

Fig. 6 Diurnal cycle of cloud cover averaged over (top) land and (bottom) ocean grid cells within the model domain for period 1998-2001 using default version of RegCM3-IBIS with

Emanuel convection scheme. Color bar indicates fractional coverage of grid cell. The x-axis labels indicate the time of the middle of each 3-hour output window, with respect to local time in the center of the model domain. To represent the y-axis on a linear scale, the vertical extent of each model layer was assigned a single value of cloud cover, as provided by the model output. In reality, a smoother profile with less abrupt vertical variability would be expected

Fig. 7 As for Figure 6 but using the modified version of RegCM3-IBIS with Emanuel convection scheme for (top) land and (bottom) ocean grid cells within the model domain

Fig. 8 Average low-level cloud fraction for 1998-2001: simulation minus ISCCP data for (a) Grell Fritsch-Chappell with default model, (b) Emanuel scheme with default model, (c) Grell scheme with modified model and (d) Emanuel scheme with modified model. Domain-averaged error (model – ISCCP cloud fraction) is shown in parentheses. Color bar indicates fractional coverage of grid cell

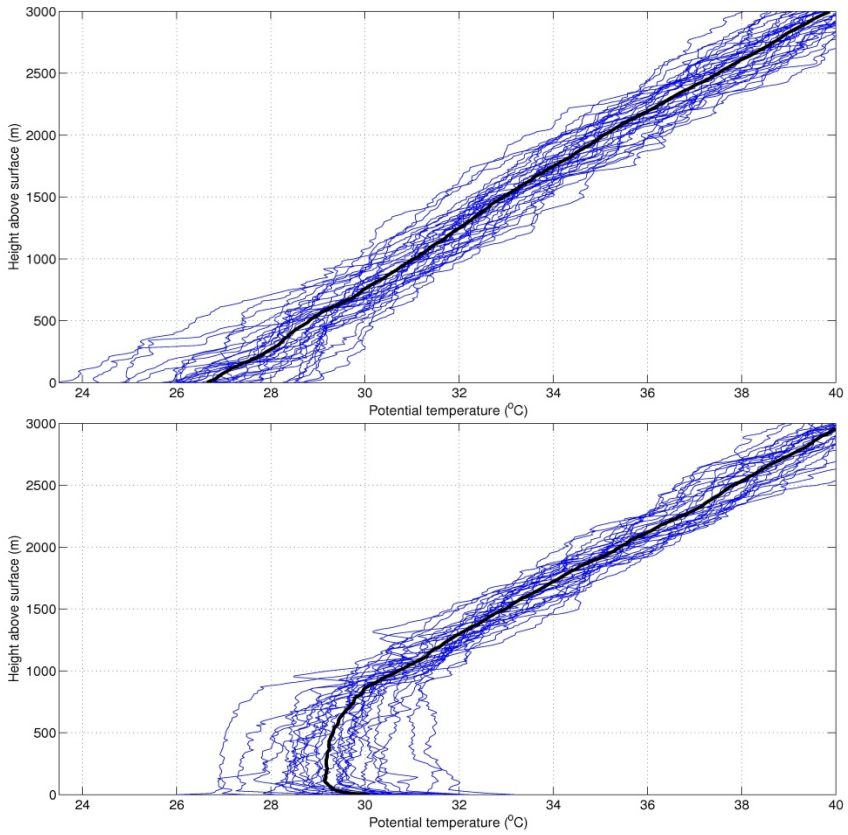
3000
2500
2000
1500
1000
500
0
Height above surface (m)
24
26
28
30
32
34
36
38
40
Potential temperature (°C)
3000
2500
2000
1500
1000
500
0
Height above surface (m)
24
26
28
30
32
34
36
38
40
Potential temperature (°C)

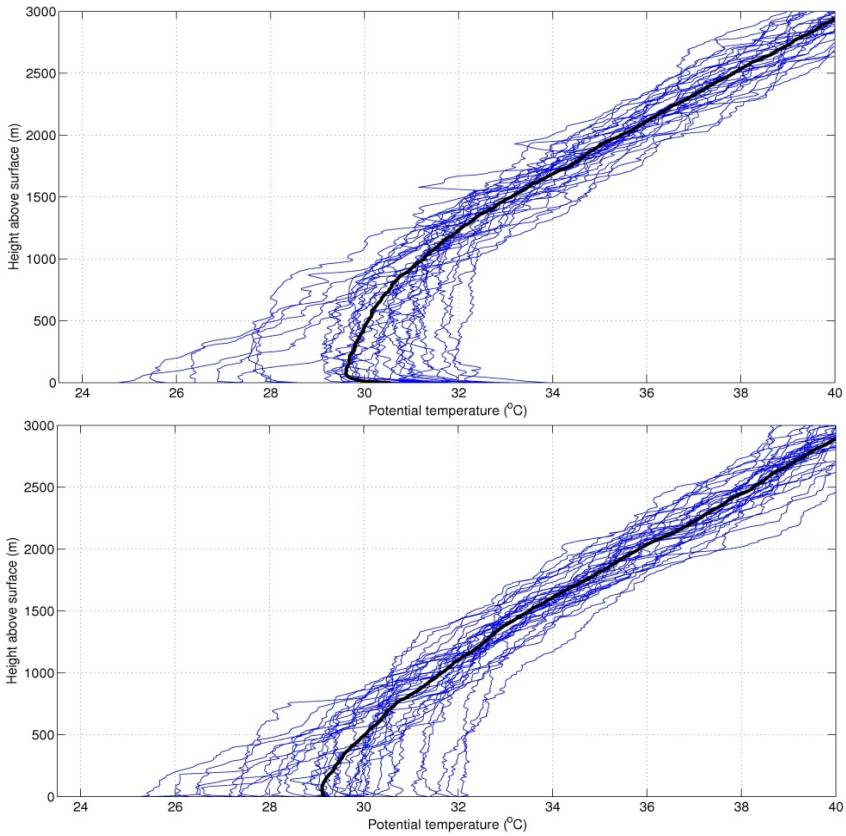

Fig. 1 Profiles of potential temperature for lowest 3 km of atmosphere from Changi Airport radiosonde data, 1 October – 23 November 2010. (a) 8 am LT; (b) 11 am LT; (c) 2 pm LT; (d) 8 pm LT. Blue lines show individual soundings; black line shows mean profile

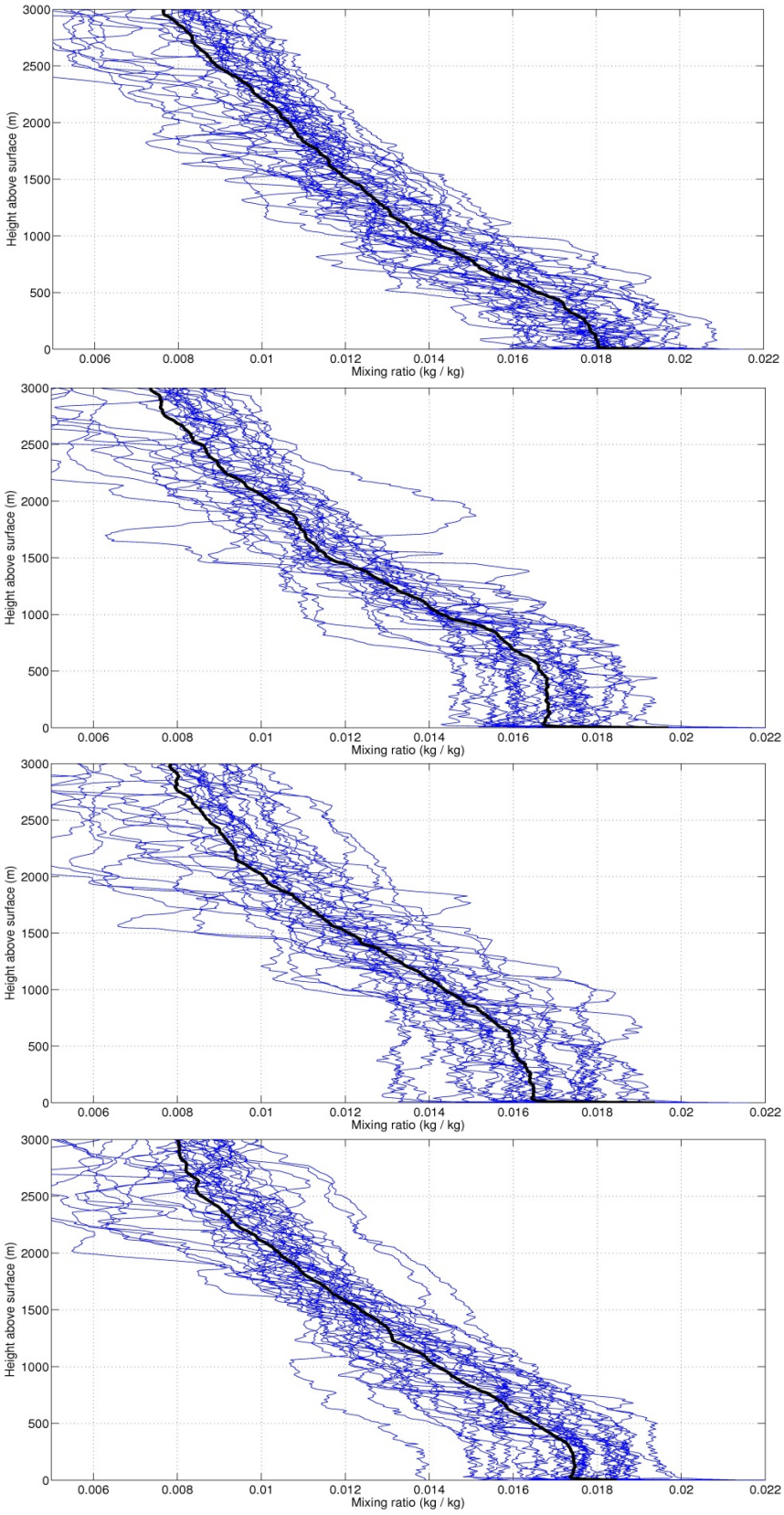
Height above surface (m)
Mixing ratio (kg / kg)
0
500
1000
1500
2000
2500
3000
0.006
0.008
0.01
0.012
0.014
0.016
0.018
0.02
0.022

Fig. 2 Profiles of water vapor mixing ratio for lowest 3 km of atmosphere from Changi Airport radiosonde data, 1 October – 23 November 2010. (a) 8 am LT; (b) 11 am LT; (c) 2 pm LT; (d) 8 pm LT. Blue lines show individual soundings; black line shows mean profile

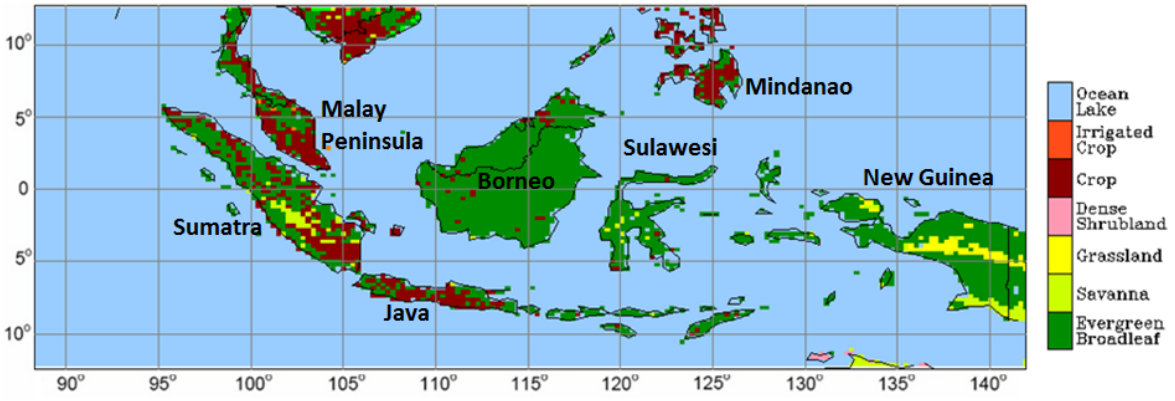

Fig. 3 Model domain showing vegetation classification used for IBIS. The domain has been sized such that it covers the generally accepted extent of the Maritime Continent region. Major islands are labeled

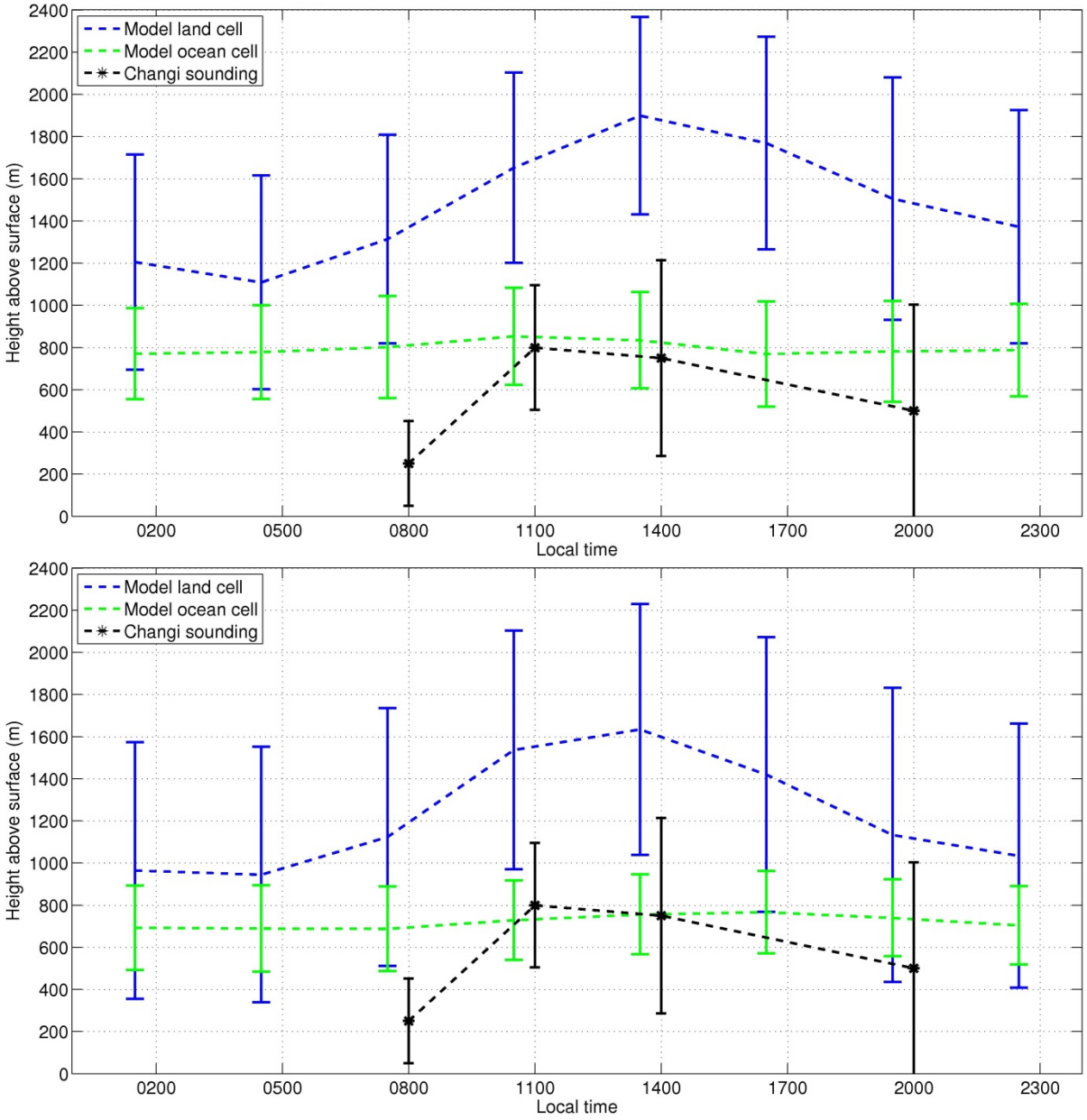

Fig. 4 Diurnal PBL height (in m) over or near Singapore, simulated by the default version of RegCM3-IBIS using (top) Grell Fritsch-Chappell and (bottom) Emanuel convection schemes using either a land (blue) or ocean (green) grid cell to represent Singapore, compared to the PBL height estimated from the Changi soundings (black stars; dashed lines are shown to interpolate between the measurement times). The vertical bars signify one standard deviation of each sample set and illustrate the variability in the simulated and observed PBL height

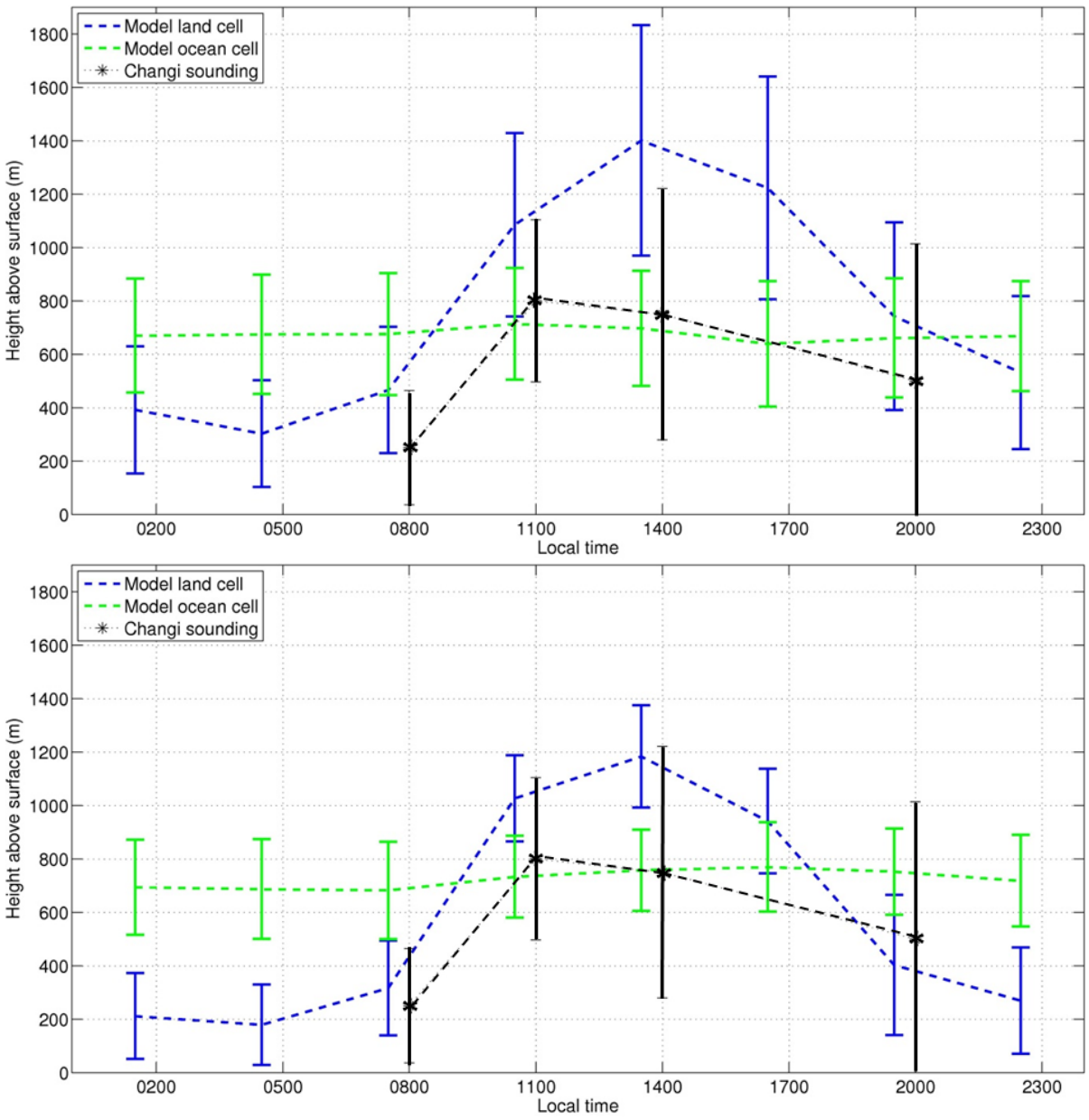

Fig. 5 As in Figure 4 but for the modified version of RegCM3-IBIS

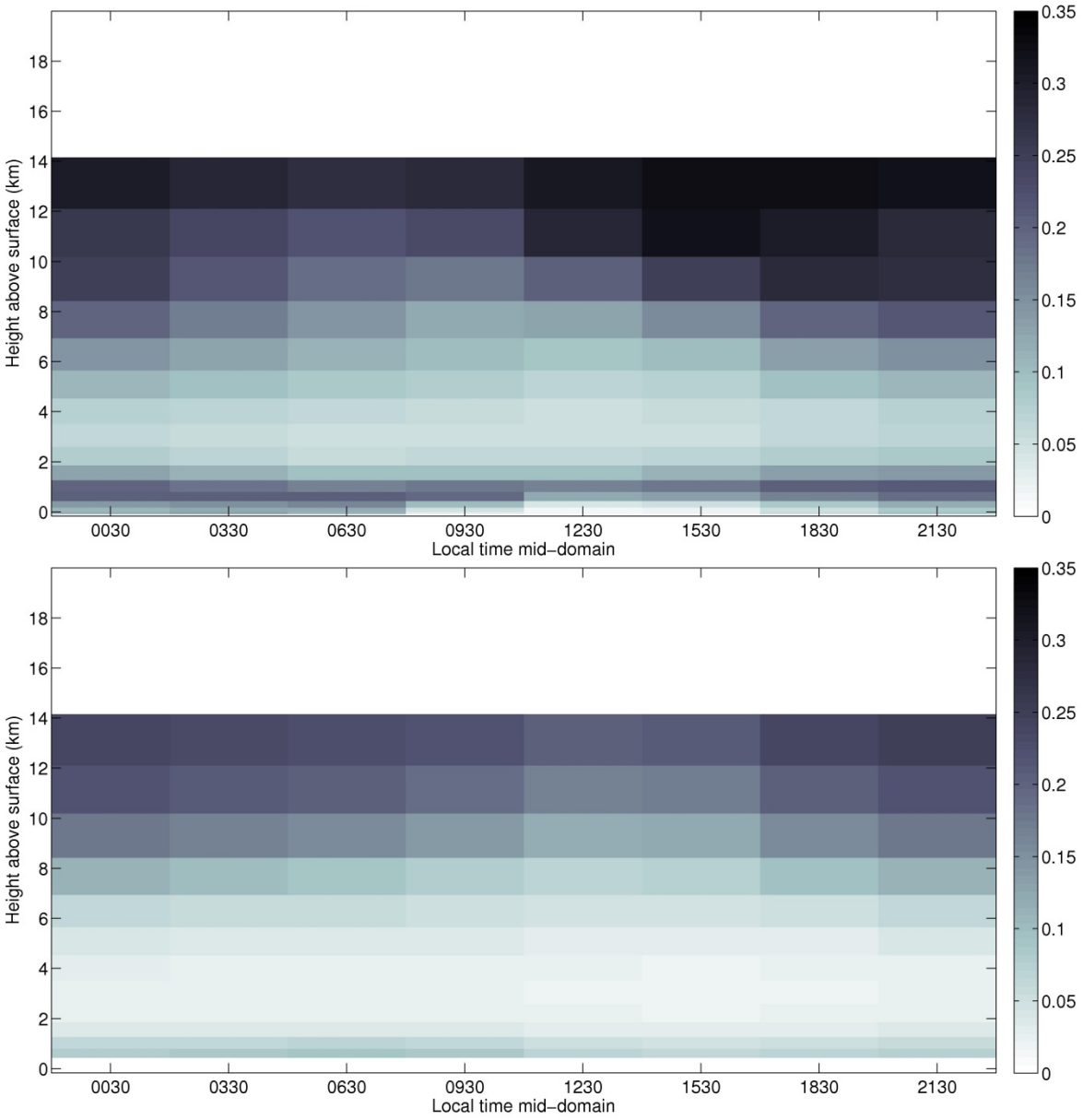

Fig. 6 Diurnal cycle of cloud cover averaged over (top) land and (bottom) ocean grid cells within the model domain for period 1998-2001 using default version of RegCM3-IBIS with Emanuel convection scheme. Color bar indicates fractional coverage of grid cell. The x-axis labels indicate the time of the middle of each 3-hour output window, with respect to local time in the center of the model domain. To represent the y-axis on a linear scale, the vertical extent of each model layer was assigned a single value of cloud cover, as provided by the model output. In reality, a smoother profile with less abrupt vertical variability would be expected

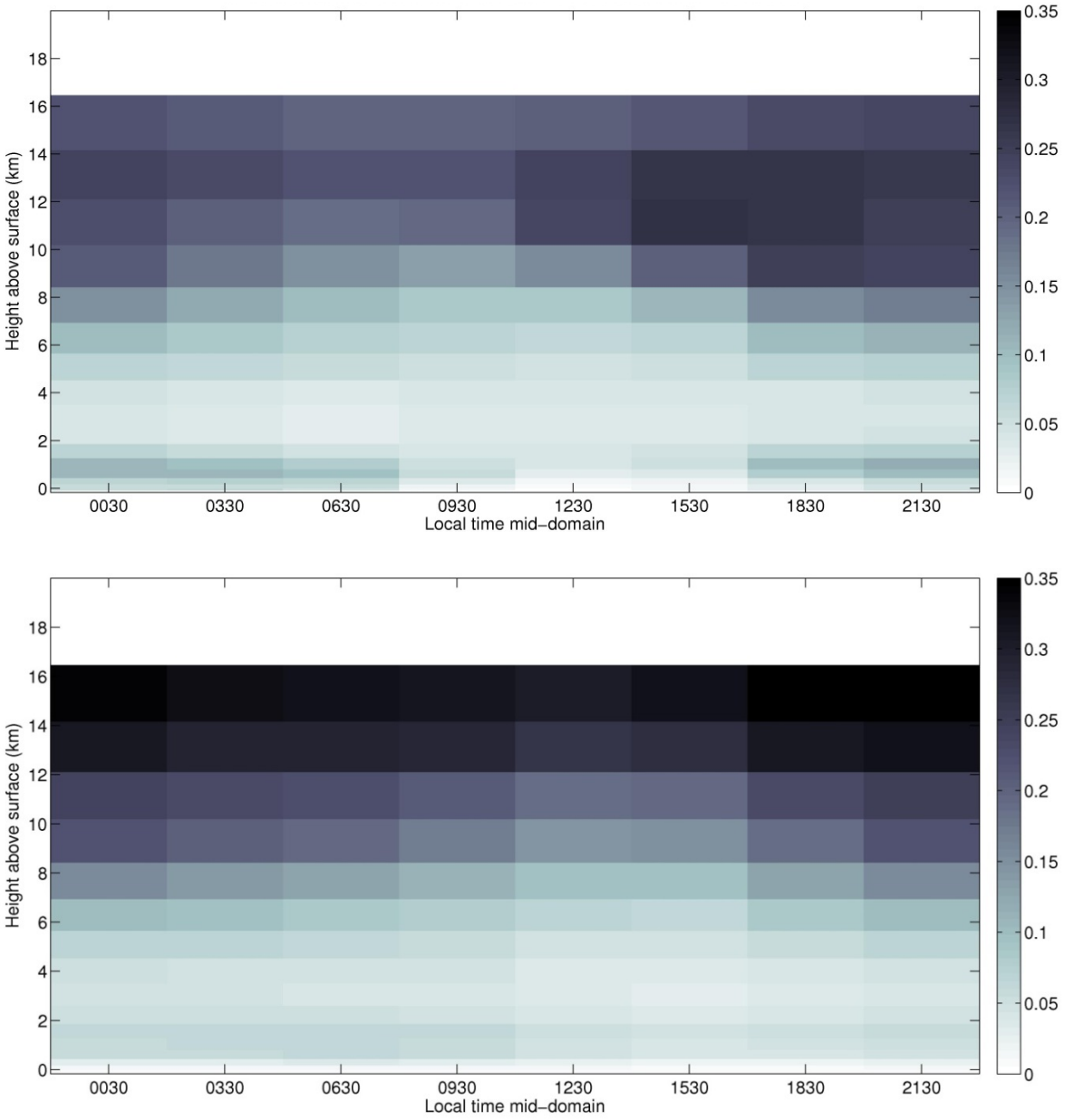

Fig. 7 As for Figure 6 but using the modified version of RegCM3-IBIS with Emanuel convection scheme for (top) land and (bottom) ocean grid cells within the model domain

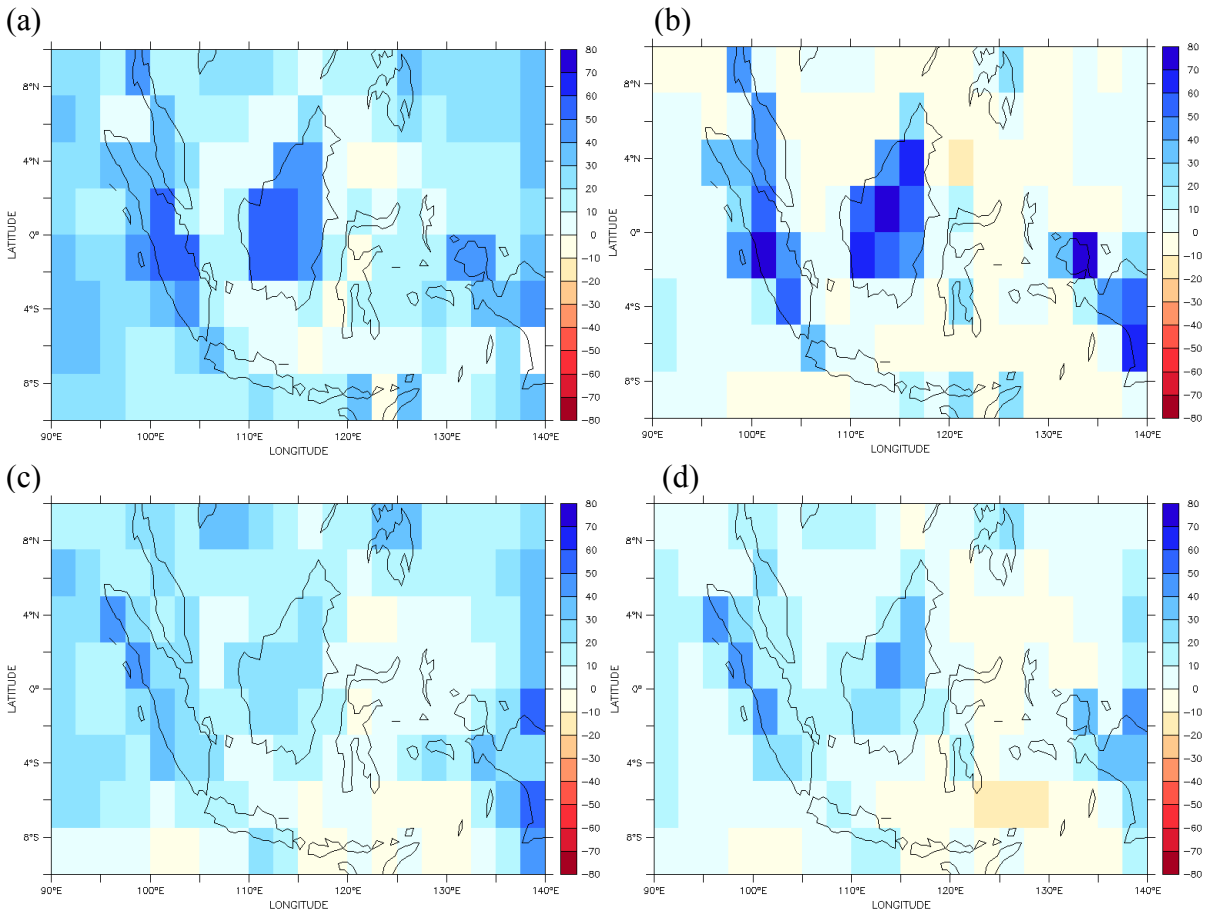

Fig. 8 Average low-level cloud fraction for 1998-2001: simulation minus ISCCP data for (a) Grell Fritsch-Chappell with default model, (b) Emanuel scheme with default model, (c) Grell scheme with modified model and (d) Emanuel scheme with modified model. Color bar indicates fractional coverage of grid cell